

Numerical errors in the computation of subfilter scalar variance in large eddy simulations

C. M. Kaul,^{1,a)} V. Raman,¹ G. Balarac,^{2,3} and H. Pitsch²

¹Department of Aerospace Engineering and Engineering Mechanics, The University of Texas at Austin, Austin, Texas 78712, USA

²Center for Turbulence Research, Stanford University, Stanford, California 94305, USA

³MOST/LEGI, BP 53, 38041 Grenoble Cedex 09, France

(Received 17 October 2008; accepted 24 March 2009; published online 14 May 2009)

Subfilter scalar variance is a key quantity for scalar mixing at the small scales of a turbulent flow and thus plays a crucial role in large eddy simulation of combustion. While prior studies have mainly focused on the physical aspects of modeling subfilter variance, the current work discusses variance models in conjunction with the numerical errors due to their implementation using finite-difference methods. *A priori* tests on data from direct numerical simulation of homogeneous turbulence are performed to evaluate the numerical implications of specific model forms. Like other subfilter quantities, such as kinetic energy, subfilter variance can be modeled according to one of two general methodologies. In the first of these, an algebraic equation relating the variance to gradients of the filtered scalar field is coupled with a dynamic procedure for coefficient estimation. Although finite-difference methods substantially underpredict the gradient of the filtered scalar field, the dynamic method is shown to mitigate this error through overestimation of the model coefficient. The second group of models utilizes a transport equation for the subfilter variance itself or for the second moment of the scalar. Here, it is shown that the model formulation based on the variance transport equation is consistently biased toward underprediction of the subfilter variance. The numerical issues in the variance transport equation stem from discrete approximations to chain-rule manipulations used to derive convection, diffusion, and production terms associated with the square of the filtered scalar. These approximations can be avoided by solving the equation for the second moment of the scalar, suggesting that model's numerical superiority. © 2009 American Institute of Physics. [DOI: 10.1063/1.3123531]

I. BACKGROUND AND MOTIVATION

Subfilter scalar variance plays a crucial role in large eddy simulation (LES) based modeling of turbulent combustion. The most popular models for nonpremixed combustion rely on a conserved scalar approach, in which a nonreactive scalar, the mixture fraction, is mapped to the thermochemical state of the fluid using a combustion model, for example, a flamelet model.^{1,2} The transport equation for the mixture fraction contains no chemical source terms, making it more tractable in the LES framework. Compared to chemically inert turbulent flows, gas-phase combustion is highly sensitive to the fine-scale distribution of the scalar. Since the filtered mixture fraction field contains no information about the small scales, additional modeling is required to statistically represent the details of scalar mixing. In one-point statistical closures, knowledge of the subfilter probability density function (PDF) allows for such a description of the scalar field.² In the context of mixture fraction, this subfilter PDF is often assumed to be a beta distribution parametrized by the filtered mixture fraction and a subfilter variance of mixture fraction.³ A subfilter variance model is required to complete the specification of the subfilter PDF.

Several models for subfilter variance have been pro-

posed in the past.⁴⁻⁷ They can be broadly divided into two categories: those based on a transport equation for the variance and those employing algebraic relations which do not account for transport of variance at resolved scales. Models in the first class are substantially holdovers from Reynolds-averaged Navier–Stokes (RANS) methodology for the mixture fraction variance. Putting aside for now the assumptions necessary to write a subfilter variance transport equation (VTE) for LES in analogy to the RANS formulations, the most pressing modeling issue for the VTE is the closure of the filtered mixture fraction dissipation rate. Within the more prevalent second class of subfilter variance models, gradient-based closures are generally found to be more accurate than other algebraic models in *a priori* studies of direct numerical simulation (DNS) data.⁸

LES computations are notoriously dependent on the numerical discretization employed for their solution.^{9,10} Given the extreme sensitivity of the entire modeled combustion process to the values of the subfilter variance, the numerical errors incurred in implementing a variance model are hardly subordinate to the innate error of the model itself. However, prior studies of model accuracy have largely failed to account for the effects of numerical scheme, and, as shown in this work, the interaction of errors often produces counterintuitive results. Below, we identify some potential numerical

^{a)}Author to whom correspondence should be addressed. Electronic mail: colleen.kaul@mail.utexas.edu.

pitfalls in variance modeling while highlighting those formulations that allow for the cancellation of finite-difference errors.

II. DESCRIPTION OF VARIANCE MODELS

LES explicitly evolves all large-scale features of a flow on a computational grid while accounting for the influence of small-scale, unresolved motions on the large scales through models. The small scales are removed using a filtering operation which can be written as

$$\bar{Z}(\mathbf{x}, t) = \int Z(\mathbf{x}', t) \mathbf{G}(\mathbf{x}' - \mathbf{x}) d\mathbf{x}', \quad (1)$$

where \bar{Z} is the filtered field corresponding to the true field $Z(\mathbf{x}, t)$ and \mathbf{G} is the three-dimensional filter kernel. The constant density case is considered for simplicity, but the numerical concerns addressed here are also applicable to variable density flows. While the filter width could be defined independently of the mesh size, grid-based implicit filtering is overwhelmingly used in practical LES calculations.¹¹ It should be noted that any useful filtered field inherently contains less information than an unfiltered field. Consequently, different realizations of the flow can produce the same filtered field.¹⁰⁻¹²

The subfilter variance is defined as

$$\begin{aligned} \bar{Z}'^2(\mathbf{x}, t) &= \int [Z(\mathbf{x}', t) - \bar{Z}(\mathbf{x}, t)]^2 \mathbf{G}(\mathbf{x}' - \mathbf{x}) d\mathbf{x}' \\ &= \bar{Z}^2(\mathbf{x}, t) - \bar{Z}^2(\mathbf{x}, t), \end{aligned} \quad (2)$$

where the first term on the right-hand side, \bar{Z}^2 , is not generally available in LES and hence needs to be modeled. For a given filtered scalar field, many different subfilter variance fields are possible. Necessarily then, all modeling is statistical. Any model can, at best, only reproduce some statistical mean of an appropriately defined ensemble.

Similar to the RANS formulation, the LES VTE can be written as

$$\begin{aligned} \frac{\partial \bar{Z}'^2}{\partial t} + \frac{\partial \bar{u}_i \bar{Z}'^2}{\partial x_i} &= \frac{\partial}{\partial x_i} \left[(D + D_t) \frac{\partial \bar{Z}'^2}{\partial x_i} \right] + 2D_t \frac{\partial \bar{Z}}{\partial x_i} \frac{\partial \bar{Z}}{\partial x_i} \\ &\quad - \left[\bar{\chi} - 2D \frac{\partial \bar{Z}}{\partial x_i} \frac{\partial \bar{Z}}{\partial x_i} \right], \end{aligned} \quad (3)$$

where eddy diffusivity models have been introduced for the scalar flux terms.⁵ In Eq. (3), u_i is the filtered velocity field and the molecular and turbulent diffusivities are denoted by D and D_t , respectively. The final bracketed term in Eq. (3) is the filtered scalar dissipation rate, where the quantity

$$\bar{\chi} = 2D \frac{\partial \bar{Z}}{\partial x_i} \frac{\partial \bar{Z}}{\partial x_i} \quad (4)$$

makes the dissipation rate an unclosed term. The methodology used in its modeling is largely informed by the approach taken in RANS. However, it must be emphasized that in RANS the mean scalar dissipation rate is a well-defined quantity that can be directly modeled, while in LES the fil-

tered scalar dissipation rate remains a random variable and any model can only try to predict some mean value. A common closure for the filtered scalar dissipation rate is

$$\bar{\chi} - 2D \frac{\partial \bar{Z}}{\partial x_i} \frac{\partial \bar{Z}}{\partial x_i} = \frac{1}{\tau} \bar{Z}'^2. \quad (5)$$

Here, τ is the scalar mixing time scale. Again, several expressions for this time scale are available. One model, based on the turbulent diffusivity and commonly used in the context of the LES/filtered-density function approach,¹³⁻¹⁵ gives

$$\tau = C_\tau \frac{\Delta^2}{D + D_t}, \quad (6)$$

where Δ is the filter width and C_τ is a model coefficient. The model coefficient does not have a universal value and depends on many parameters, including the distribution of the resolved length scales and the location of the filter cutoff in the scalar energy spectrum. The sensitivity of the coefficient to so many factors and the importance of the coefficient in determining the dissipation rate are some of the more obvious weaknesses of the VTE in terms of physical modeling.⁵ In addition, the evaluation of the production term,

$$\mathcal{P} = 2D_t \frac{\partial \bar{Z}}{\partial x_i} \frac{\partial \bar{Z}}{\partial x_i}, \quad (7)$$

which appears on the right-hand side of the VTE model, is problematic from a numerical perspective because of its gradient-squared dependency, as explained in Sec. IV A.

An alternative formulation is based on the transport equation for the second moment of the mixture fraction, which will be referred to as the STE model. The \bar{Z}^2 equation can be written as

$$\frac{\partial \bar{Z}^2}{\partial t} + \frac{\partial \bar{u}_i \bar{Z}^2}{\partial x_i} = \frac{\partial}{\partial x_i} \left[(D + D_t) \frac{\partial \bar{Z}^2}{\partial x_i} \right] - \bar{\chi} \quad (8)$$

and the subfilter variance can then be calculated using Eq. (2). Note that the modeling of $\bar{\chi}$ is a key bottleneck in using either the STE or VTE model.

Models of the second class considered here, which are algebraic in form, do not account for the transport of scalar variance by the large scales of the flow. This approximation is usually referred to as the local equilibrium approximation.¹⁶ Essentially, the production and dissipation of scalar energy are assumed to be locally balanced. Since production and dissipation are both random fields, their instantaneous values are, in general, not equivalent. Rather, the equilibrium is implied to hold for their mean values.

The local equilibrium assumption, combined with an eddy diffusivity model for the subfilter flux, allows the filtered scalar dissipation rate to be expressed as¹⁷

$$\bar{\chi} - 2D \frac{\partial \bar{Z}}{\partial x_i} \frac{\partial \bar{Z}}{\partial x_i} = 2D_t \frac{\partial \bar{Z}}{\partial x_i} \frac{\partial \bar{Z}}{\partial x_i}. \quad (9)$$

If the filtered scalar dissipation rate is then modeled using Eq. (5), the algebraic relation

$$\overline{Z'^2} = C\Delta^2 \frac{\partial \overline{Z}}{\partial x_i} \frac{\partial \overline{Z}}{\partial x_i}, \quad (10)$$

where $C=2/C_\tau$ results. The constant C still needs to be determined and is commonly obtained through a dynamic modeling procedure. Using two forms, taken to be equivalent, for the scalar energy between the LES filter scale and some larger test filter scale, an algebraic closure for the model constant can be found.⁶ Letting $\widehat{(\cdot)}$ denote a test filtered quantity, with $\hat{\Delta}$ the test filter width, the dynamic model can be written as

$$\widehat{\overline{Z}^2} - \widehat{\overline{Z}}^2 = C_1 \Delta^2 \left[\left(\frac{\hat{\Delta}}{\Delta} \right)^2 \nabla \widehat{\overline{Z}} \cdot \nabla \widehat{\overline{Z}} - \widehat{\nabla \overline{Z} \cdot \nabla \overline{Z}} \right]. \quad (11)$$

This classic dynamic model, hereafter referred to as CDM, has been widely used in combustion LES. Recently, Balarac *et al.*⁷ showed that the CDM formulation ignores certain leading-order terms in the Taylor series expansion of the left-hand side of the dynamic closure, often called the Leonard term \mathcal{L} . They proposed an alternative model (henceforth, BPR) for which the dynamic closure is written as

$$\widehat{\overline{Z}^2} - \widehat{\overline{Z}}^2 = C_2 \hat{\Delta}^2 \nabla \widehat{\overline{Z}} \cdot \nabla \widehat{\overline{Z}}. \quad (12)$$

While other algebraic variance models are available,⁴ the dynamic procedure obviates the need to specify the model coefficient *a priori* and is therefore the top choice for combustion modeling.^{6,8} If transport or accumulation of variance cannot be neglected, then either the VTE model [Eq. (3)] or the STE model [Eq. (8)] must be used, with the caveat that $\bar{\chi}$ has to be modeled.

It is important to note that the subfilter scalar variance has most of its energy content in the largest subfilter scales and is therefore in the algebraic models estimated from the smallest filtered scales, which are identified using the test filtering operation. Similarly, the production term appearing in the scalar variance equation actually describes an energy cascade process, in which energy is transferred from the smallest filtered scales to the largest subfilter scales. In both cases, the smallest filtered scales are of significance. Because the filter width and grid spacing are equal in implicit LES, these scales are not resolved properly. It can be expected that numerical errors in terms involving the smallest filtered scales are of leading order. Therefore, the models cannot be considered apart from these errors. With this context in mind, the interaction of discretization errors with the models is discussed below. First, the dynamic model is considered and a simplified scalar field is analyzed in order to demonstrate its error cancellation effect. This behavior is then validated using DNS of homogeneous isotropic turbulence. Turning next to the transport equation models, sources of error in the VTE model are examined and the behavior of the STE model is discussed.

III. MODIFIED WAVE NUMBER ANALYSIS

A modified wave number analysis^{18,19} can be used to illustrate the effect of numerical errors on model prediction. Consider a filtered scalar field represented by a single wave-mode,

$$\overline{Z}(x) = e^{ikx}, \quad (13)$$

where k is some specific wave number and x is the physical coordinate. To compute the model coefficient in the dynamic model, a test filtering operation is necessary. For explicitness, the filtering kernel is assumed to be a top-hat function with step size of $\hat{\Delta}$, which also refers to the test filter width. Then

$$\widehat{\overline{Z}} = \frac{1}{\hat{\Delta}} \int_{x-\hat{\Delta}/2}^{x+\hat{\Delta}/2} \overline{Z}(x') dx' = \frac{2}{\hat{\Delta}k} \sin(k\hat{\Delta}/2) e^{ikx} = f(k) e^{ikx}. \quad (14)$$

The test filtering operation can be represented as multiplication by a function of the wave number, which modulates the amplitude of a mode but does not affect the wave number associated with it.

For notational convenience, an operator \mathcal{G} operating on a field H is defined as

$$\mathcal{G}(H) \equiv \nabla H \cdot \nabla H. \quad (15)$$

The dynamic model for the coefficient C_1 can be written as

$$\mathcal{L} = C_1 \mathcal{M}, \quad (16)$$

where the model terms, specialized to our example function, are

$$\mathcal{L} = \widehat{\overline{Z}^2} - \widehat{\overline{Z}}^2 = e^{i2kx} [f(2k) - f^2(k)] \quad (17)$$

and

$$\mathcal{M} = \Delta^2 [p^2 \mathcal{G}(\widehat{\overline{Z}}) - \widehat{\mathcal{G}(\overline{Z})}] = -k^2 \Delta^2 e^{i2kx} [p^2 f^2(k) - f(2k)]. \quad (18)$$

Here, Δ is the width of the filter used to obtain \overline{Z} and $p = \hat{\Delta}/\Delta$ denotes the ratio of the test filter width to the LES filter width. To enhance the stability of the simulation, C_1 is typically calculated by averaging over homogeneous directions,⁶ that is,

$$C_1 = \frac{\langle \mathcal{L} \mathcal{M} \rangle}{\langle \mathcal{M}^2 \rangle}. \quad (19)$$

For this special case, the direct division \mathcal{L}/\mathcal{M} and the averaging procedure expressed by Eq. (19) produce identical results:

$$C_1 = \frac{f(2k) - f^2(k)}{-\Delta^2 k^2 [p^2 f^2(k) - f(2k)]}. \quad (20)$$

The subfilter variance for this scalar field is evaluated as

$$\overline{Z'}^{\text{ideal}} = C_1 \Delta^2 \mathcal{G}(\overline{Z}) = \frac{f(2k) - f^2(k)}{p^2 f^2(k) - f(2k)} e^{i2kx}. \quad (21)$$

It should be noted that for the chosen test field, the variance depends on the type of filter used (which determines the form of f) and the test filter width used (which determines p).

While the exact derivative for the test function defined in Eq. (13) is given by $d\overline{Z}/dx = ike^{ikx}$, finite-difference operators produce a different value. For a given scheme and fixed grid spacing h , the error depends only on the wave number of the function being differentiated and can be expressed in terms of a modified wave number g . Thus, the derivative evaluated using a finite-difference scheme is given by

$$\frac{d\overline{Z}^{\text{fd}}}{dx} = ig(k)e^{ikx}. \quad (22)$$

For the central schemes that will be considered here, g assumes only real values so that the error is manifested solely in the amplitude of the derivative. In Eq. (22), obviously the scheme is exact if $g(k)$ tends to k , which is the case if the wave number or the grid spacing tends to zero. However, for larger values of k , the modified wave number becomes small, resulting in a large error. For a second-order central difference scheme, $g(k) = \sin(kh)/h$. Modified wave numbers for other schemes are available in the literature.¹⁹ The finite-difference operator for \mathcal{G} is denoted by \mathcal{G}^{fd} , e.g., $\mathcal{G}^{\text{fd}}(\overline{Z}) = -g^2(k)e^{i2kx}$. Using finite-difference operators does not affect the values of \mathcal{L} , but \mathcal{M} is replaced by

$$\begin{aligned} \mathcal{M}^{\text{fd}} &= \Delta^2 [p^2 \mathcal{G}^{\text{fd}}(\hat{\overline{Z}}) - \widehat{\mathcal{G}^{\text{fd}}(\overline{Z})}] \\ &= -g^2(k) \Delta^2 e^{i2kx} [p^2 f^2(k) - f(2k)]. \end{aligned} \quad (23)$$

Using the finite-difference operation defined in Eq. (22) and the test filtering operation defined in Eq. (13) and averaging as in Eq. (19), the dynamic model coefficient evaluates as

$$C_1^{\text{fd}} = \frac{f(2k) - f^2(k)}{-\Delta^2 g^2(k) [p^2 f^2(k) - f(2k)]}. \quad (24)$$

Comparing this result with Eq. (20) shows that the ratio of the exact model coefficient to the finite-difference value is $[k/g(k)]^2$. As discussed earlier, the smallest resolved scales in LES will dominate the model evaluation. The function $g(k)$ is always less than k for nonzero grid spacing, implying that there is an inherent overprediction of the model coefficient due to the use of a finite-difference scheme. However, the variance evaluated with the coefficient from Eq. (24) is

$$\overline{Z'}^{\text{fd}}_{\text{CDM}} = C_1^{\text{fd}} \Delta^2 \mathcal{G}^{\text{fd}}(\overline{Z}) = \frac{f(2k) - f^2(k)}{p^2 f^2(k) - f(2k)} e^{i2kx} = \overline{Z'}^{\text{ideal}}_{\text{CDM}}. \quad (25)$$

Although the coefficient is overpredicted, the finite-difference approximation does not affect the predicted variance. This result is explained by noting that the filtering and finite-differencing operations do not modify the wave number associated with the field but rather act only to damp the amplitude of the mode. The final step in computing the vari-

ance [Eq. (25)] cancels the damping error, thereby eliminating the effect of the finite-difference operator. This result, for the case of a scalar field containing a single wavemode, is independent of the finite-difference approximation used and is valid for any filter kernel that does not generate additional modes.

Proceeding along similar lines, it can be shown that the BPR dynamic procedure, when applied to a unimodal scalar field, is also insensitive to finite-difference error. As in the finite-difference CDM model, overprediction of the model coefficient is exactly compensated for by underprediction of \mathcal{G}^{fd} , so that

$$\overline{Z'}^{\text{fd}}_{\text{BPR}} = \frac{f(2k) - f^2(k)}{p^2 f^2(k)} e^{i2kx} = \overline{Z'}^{\text{ideal}}_{\text{BPR}}. \quad (26)$$

In realistic turbulent flows, many different wavemodes exist. Consequently, a simple analysis like the one carried out above is not possible. Even if only two wavemodes are present, the numerical error associated with the dynamic procedure plays a nontrivial role. The results of the simplified case are, however, quite suggestive. While \mathcal{G}^{fd} is inevitably underpredicted when high wave number modes (i.e., scales just greater than the filter width) are present, overprediction of the model coefficient due to the dynamic procedure would ostensibly reduce the total error in the variance calculation. Next, DNS-based *a priori* tests are conducted to assess the dynamic models' error-mitigating effects in a realistic flow.

IV. DNS-BASED A PRIORI ANALYSIS OF NUMERICAL ERRORS

A pseudospectral code was used to compute forced isotropic turbulence in a periodic domain. The velocity field was forced by introducing energy at the large wave numbers.²⁰ The scalar field was allowed to decay from an initially segregated state.²¹ The computation was carried out on a 512^3 grid using 128 processors. At steady state, Re_λ was roughly 135. The Schmidt number was set to unity. The code has been verified and validated using canonical flow configurations and using theoretical correlations for the higher-order statistics. All the analyses in this section are based on this data set. A box filter was used throughout for LES and test filtering. In similar tests by Balarac *et al.*,⁷ the use of a Gaussian filter was shown to have no significant effect on the results. The ratio of test to LES filter widths ($\hat{\Delta}/\Delta$) was held at 2.

A. Effect of discretization errors on the dynamic model

For this study, three different numerical schemes, namely, the second-order central difference (CD-2), fourth-order central difference (CD-4), and sixth-order Padé (Padé-6) schemes, are considered. The discretization schemes are emulated using the corresponding modified wave number.^{18,19} The dynamic model is built on a gradient-based scaling law that requires the computation of the square of the scalar gradient. To understand the impact of discretization, the scalar gradient-squared field computed using

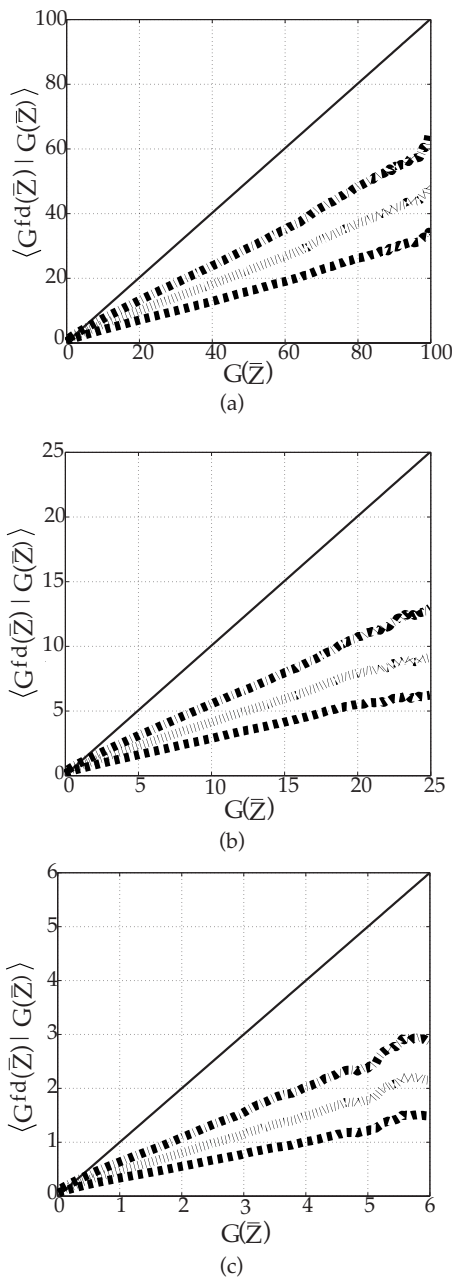


FIG. 1. Plot of the conditional average of the gradient-squared term, $G^{fd}(\bar{Z})$, computed using various finite-difference approximations: (dashed line) CD-2, (dotted line) CD-4, and (dashed-dotted line) Padé-6 schemes. The conditioning variable is the spectrally computed $G(\bar{Z})$. The three plots correspond to three different filter sizes: (a) $\Delta = 16\eta$, (b) $\Delta = 32\eta$, and (c) $\Delta = 64\eta$, where η is the Kolmogorov length scale.

finite-difference approximations, $G^{fd}(\bar{Z})$, should first be compared to the term computed using a spectral method, $G(\bar{Z})$.

Figure 1 shows the conditional average of the finite-difference approximation conditioned on the spectrally computed gradient-squared term plotted for different filter sizes. The mesh size is taken to be equal to the filter width. Clearly, the finite-difference methods underpredict the gradient-squared term. As the order of the scheme decreases, the errors increase, which is consistent with basic theory for the order of accuracy of finite-difference schemes. It can also be seen that the magnitudes of the DNS-based gradients de-

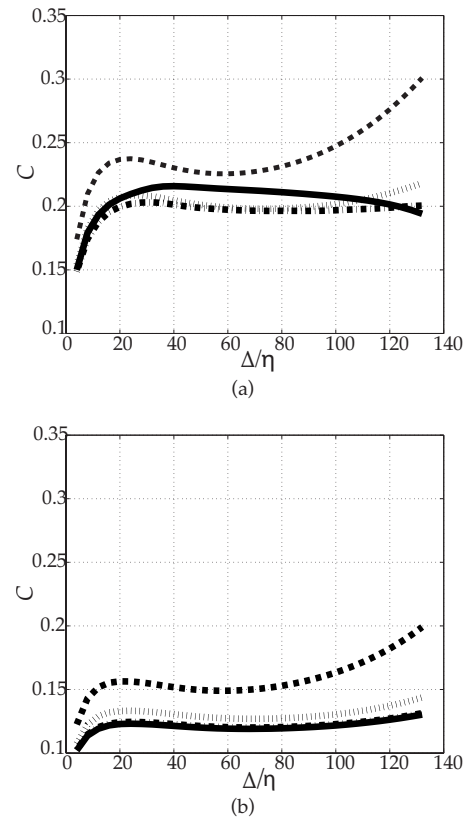


FIG. 2. Dynamic model coefficient for (a) CDM and (b) BPR. The coefficient is computed by averaging over the entire computational domain. $\langle Z'^2 \rangle = 0.1802$. Results for (solid line) spectral, (dashed line) CD-2, (dotted line) CD-4, and (dashed-dotted line) Padé-6 schemes are shown.

crease with increasing filter width and, while the absolute magnitudes of the finite-difference errors also decrease, the relative errors become greater. It is important to note that as the filter width increases, the true subfilter variance will also increase, reflecting larger amounts of unresolved scalar energy. If the scalar gradient is underpredicted, the model coefficient should correspondingly increase in order to predict the variance correctly. Additionally, the range of scalar gradient values will narrow as the scalar field evolves. An indication of the variability of the scalar field is given by the global variance $\langle Z'^2 \rangle = \langle Z^2 \rangle - \langle Z \rangle^2$, where $\langle \cdot \rangle$ denotes an average taken over the entire volume. It is then not surprising that the results of the dynamic model change as the scalar becomes more mixed, which is represented by a decrease in the value of $\langle Z'^2 \rangle$.

Figures 2 and 3 show the model coefficients computed using the classic model (CDM) and the improved model (BPR) at two different times. Several key points have to be noted. First, the choice of numerical method clearly impacts the value of the coefficients computed. As the order of the scheme is increased, the coefficient value at any filter size decreases. This in itself indicates that the dynamic procedure will mitigate some of the gradient underprediction discussed above. Second, the Padé scheme performs very similarly to the spectral scheme in calculating the BPR model coefficient for both scalar fields. Third, the CDM coefficient has very peculiar behavior. The spectrally computed CDM coefficient

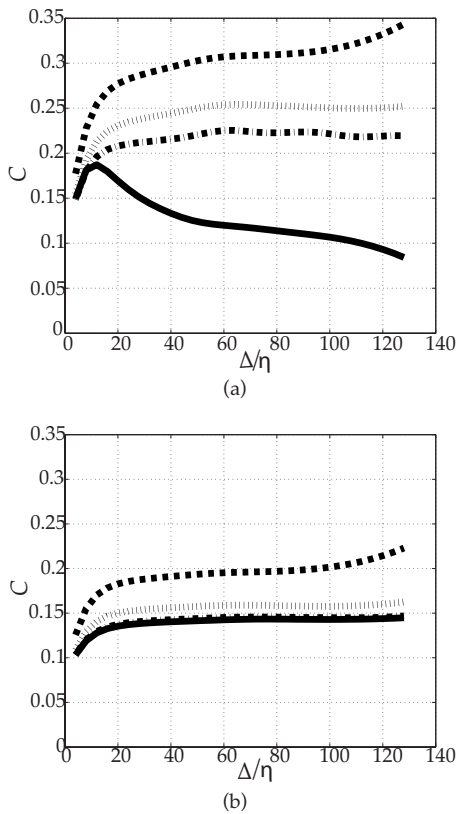


FIG. 3. Dynamic model coefficient for (a) CDM and (b) BPR. The coefficient is computed by averaging over the entire computational domain. $\langle Z'^2 \rangle = 0.1015$. Results for (solid line) spectral, (dashed line) CD-2, (dotted line) CD-4, and (dashed-dotted line) Padé-6 schemes are shown.

first increases then begins to drop with increasing filter width. The fall-off of the spectral coefficient value steepens as $\langle Z'^2 \rangle$ decreases and the peak value occurs at a smaller filter width. As pointed out by Balarac *et al.*,⁷ the declining value is due to the large negative correlation between the \mathcal{L} and \mathcal{M} terms in the model evaluation. None of the finite-difference approximations appear to capture this correlation well, thereby leading to a marked difference in the trends. Instead, the finite-difference CDM coefficients seem to follow a trend similar to the BPR model coefficient. As the global variance decreases, the magnitude of the BPR coefficient increases for all schemes, but the variations between the schemes remain quite similar.

Figures 4 and 5 show the quadratic error between the modeled variance and the DNS subfilter variance for a range of filter widths. This error is defined as

$$\text{error} = \frac{\langle (\overline{Z'^2}_{\text{model}} - \overline{Z'^2}_{\text{DNS}})^2 \rangle}{\langle \overline{Z'^2}_{\text{DNS}} \rangle^2}. \quad (27)$$

Interestingly, the discretization order has a limited impact on the variance prediction. Regardless of the model used, the errors associated with the evaluation of the gradients are compensated for by the errors in the dynamically calculated model coefficient, which is consistent with the results of the modified wave number analysis presented in Sec. III. While the higher-order schemes show marginal improvement, the second-order scheme is surprisingly accurate in predicting

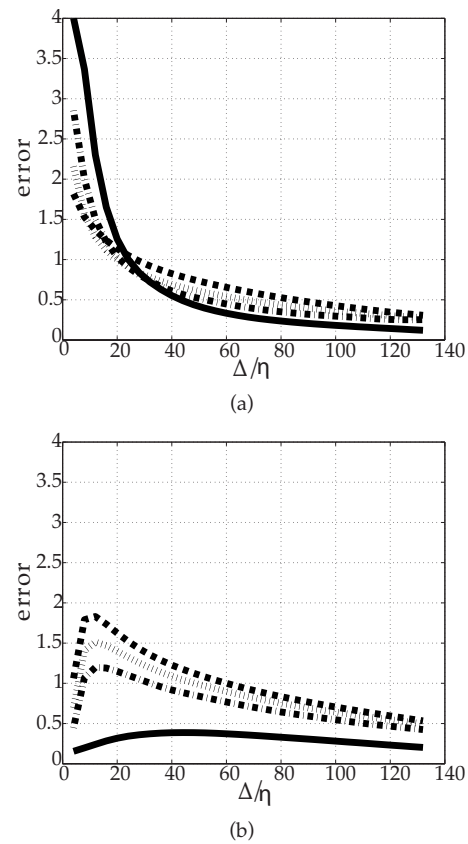


FIG. 4. Quadratic error generated by (a) CDM and (b) BPR model, calculated by (solid line) spectral, (dashed line) CD-2, (dotted line) CD-4, and (dashed-dotted line) Padé-6 schemes in relation to the true variance. $\langle Z'^2 \rangle = 0.1802$.

the variance. It can also be observed that, despite the BPR model's lower modeling error (evidenced by the lower error of its spectral form), finite-difference approximations of the BPR model do not necessarily perform better than the corresponding CDM implementations. However, the BPR model exhibits well-defined behavior in terms of reduced error for higher-order numerics over the whole range of filter widths. For both scalar fields, the finite-difference CDM formulations perform worst at smaller filter widths but monotonically improve in accuracy as the filter width increases. However, the trend in the error for the spectrally computed CDM variance changes with $\langle Z'^2 \rangle$. The error shows a steady decrease with increasing filter width at the higher global variance. At the lower value of global variance, the error shows a distinct minimum at about $\Delta = 20\eta$ and then increases with filter width. A similar phenomenon occurs for the spectrally computed BPR model.

These analyses demonstrate that variance modeling using a gradient-based scaling law is subject to significant finite-differencing errors. The presence of a range of wave numbers in a turbulent flow leads to complex, nonlinear interactions within dynamic gradient-based models, producing results that fail to follow conventional error convergence estimates. In particular, there is no guarantee that higher-order schemes will incur less error, at least in the case of the original dynamic procedure.

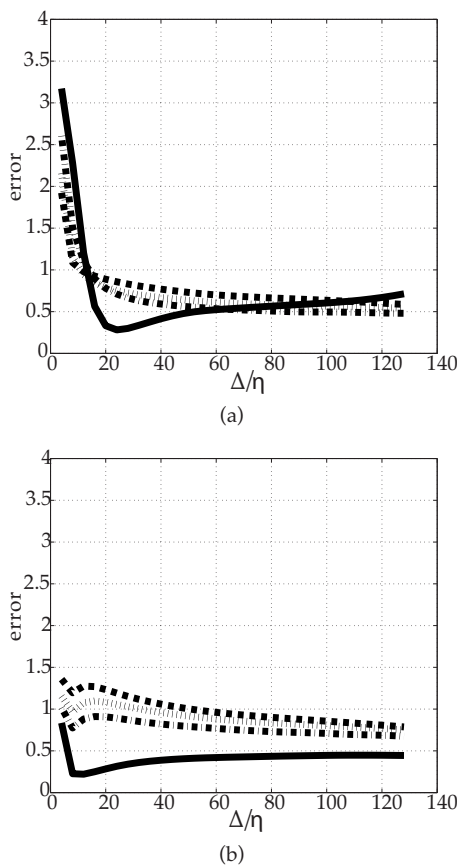


FIG. 5. Quadratic error generated by (a) CDM and (b) BPR model, calculated by (solid line) spectral, (dashed line) CD-2, (dotted line) CD-4, and (dashed-dotted line) Padé-6 schemes in relation to the true variance. $\langle Z'^2 \rangle = 0.1015$.

B. Transport equation based models for variance

An alternate approach for modeling variance is based on solving a transport equation. This transport equation could evolve either the scalar variance [VTE model, Eq. (3)] or the second moment of the scalar [STE model, Eq. (8)]. In this section, we demonstrate that the VTE model has significant numerical errors in convection, diffusion, and production terms associated with \bar{Z}^2 , which do not appear in the STE model. The STE formulation is therefore superior to the VTE model.

The primary advantage of the STE formulation is its ability to recover the analytical solution for variance in the absence of scalar dissipation. For the sake of this discussion, we set the term $\bar{\chi}$ in Eq. (8) to zero. Then, the mixture fraction transport equation and the STE are identical in form. In all practical computations, the variance of mixture fraction at the inflow boundaries and walls is set to zero. In this case, the mixture fraction equation and the STE will evolve identically. In other words, $\bar{Z}^2 = \bar{Z}$ at all spatial locations and for all times. This also implies that the variance is a function only of the filtered mixture fraction, everywhere assuming its local maximum value since

$$\bar{Z}'^2 = \bar{Z}^2 - \bar{Z}^2 = \bar{Z} - \bar{Z}^2 = \bar{Z}(1 - \bar{Z}). \quad (28)$$

The STE model then reproduces the correct variance trivially by virtue of the formulation.

The VTE approach, on the other hand, does not possess this feature. Starting from the definition of subfilter variance [Eq. (2)], the temporal evolution of variance can be written as

$$\frac{d\bar{Z}'^2}{dt} = \frac{d\bar{Z}^2}{dt} - \frac{d\bar{Z}^2}{dt}. \quad (29)$$

The first term on the right-hand side is the second moment transport equation or the STE model [Eq. (8)]. The second term evolves \bar{Z}^2 , which is redundant because the equation for \bar{Z} is already being solved. The second term has to be expressed in terms of the filtered mixture fraction transport equation by application of the chain rule. However, forms which are equivalent for continuous variables are not equal in the discrete case, i.e.,

$$\frac{\delta \bar{Z}^2}{\delta t} \neq 2\bar{Z} \frac{\delta \bar{Z}}{\delta t}, \quad (30)$$

where the operator δ refers to the finite-difference approximation of the transport equation. To further understand the numerical errors, the individual transport terms of the \bar{Z}^2 equation need to be studied and compared to the terms of the $2\bar{Z}\delta\bar{Z}/\delta t$ equation. We define the following quantities for this purpose:

$$P_1 = 2\bar{Z} \frac{\delta \bar{u}_j \bar{Z}}{\delta x_j}, \quad P_2 = \frac{\delta \bar{u}_j \bar{Z}^2}{\delta x_j}, \quad (31)$$

and

$$Q_1 = 2\bar{Z} \frac{\delta}{\delta x_j} \left[(D + D_t) \frac{\delta \bar{Z}}{\delta x_j} \right], \quad (32)$$

$$Q_2 = \frac{\delta}{\delta x_j} \left[(D + D_t) \frac{\delta \bar{Z}^2}{\delta x_j} \right] - 2(D + D_t) \frac{\delta \bar{Z}}{\delta x_j} \frac{\delta \bar{Z}}{\delta x_j}.$$

P_1 and Q_1 are the discrete versions of the convection and diffusion terms, respectively, in the $2\bar{Z}\delta\bar{Z}/\delta t$ equation, while P_2 and Q_2 are the corresponding terms of the discrete \bar{Z}^2 equation. Note that the second term in Q_2 includes the production term in the scalar variance equation.

Using these definitions, the transport equations for $2\bar{Z}\delta\bar{Z}/\delta t$ and $\delta\bar{Z}^2/\delta t$ can be written in semidiscretized form as

$$2\bar{Z} \frac{\delta \bar{Z}}{\delta t} = -P_1 + Q_1 \quad (33)$$

and

$$\frac{\delta \bar{Z}^2}{\delta t} = -P_2 + Q_2. \quad (34)$$

It should be recalled that to obtain an equation for the variance, Eq. (34) must be subtracted from the transport equation for \bar{Z}^2 , but only Eq. (33) is known in the context of the filtered scalar transport equation. The error is hence expressed in the differences between P_1 , P_2 and Q_1 , Q_2 .

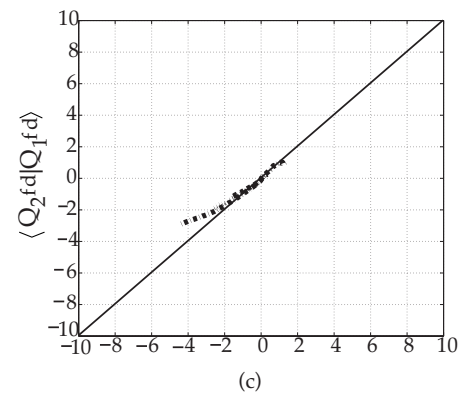
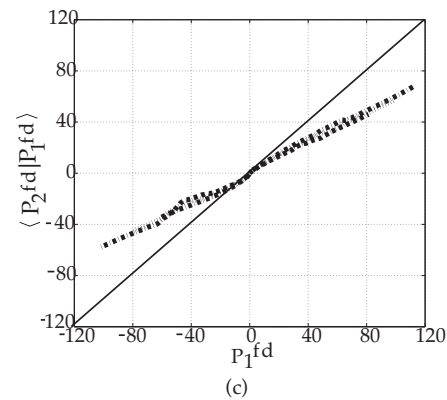
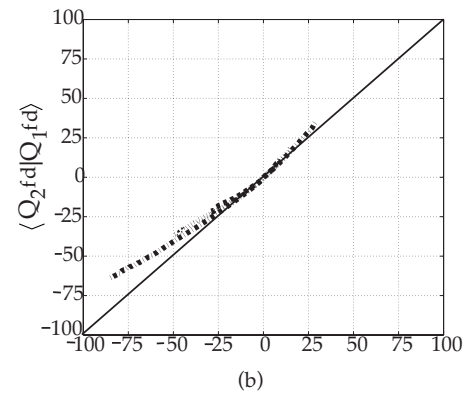
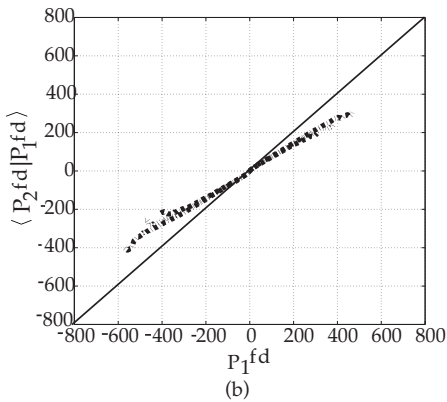
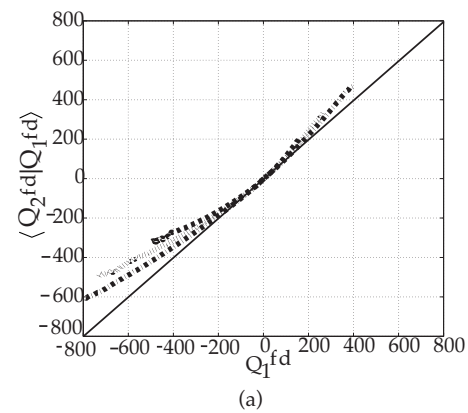
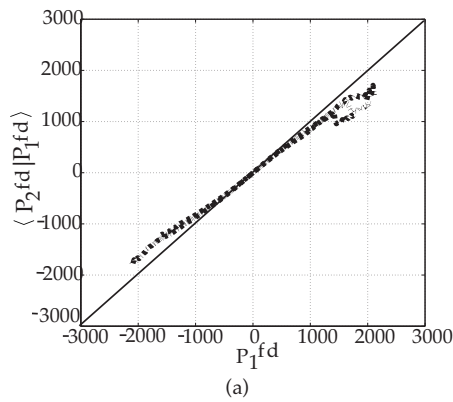


FIG. 6. Conditional mean $\langle P_2 | P_1 \rangle$ plotted for filter widths of (a) 8η , (b) 32η , and (c) 128η using different numerical schemes: (dashed line) CD-2, (dotted line) CD-4, and (dashed-dotted line) Padé-6.

FIG. 7. Conditional mean $\langle Q_2 | Q_1 \rangle$ plotted for filter widths of (a) 8η , (b) 32η , and (c) 128η using different numerical schemes: (dashed line) CD-2, (dotted line) CD-4, and (dashed-dotted line) Padé-6.

For the purpose of comparison, consider the conditional mean quantities, $\langle P_2 | P_1 \rangle$ and $\langle Q_2 | Q_1 \rangle$. The departures of these quantities from P_1 and Q_1 , respectively, provide an estimate of the errors induced by the chain-rule approximation encapsulated in Eq. (30). Figures 6 and 7 show the conditional mean values evaluated for a range of filter sizes. The turbulent diffusivity was obtained using a dynamic procedure.²² The plots reveal some interesting trends. The $\langle P_2 | P_1 \rangle$ term is overpredicted when the P_1 term is negative and underpredicted when P_1 is positive, so that the magnitude of P_1 is always underpredicted. The P terms are flux terms so errors in their values affect the redistribution of variance.

The term $\langle Q_2 | Q_1 \rangle$ behaves differently from the convection term. The chain-rule approximation seems to affect the

negative terms more than the positive terms. For all filter widths, the conditional mean lies above the diagonal, indicating that the Q_2 term is generally overpredicted. However, the error is more pronounced when Q_1 is negative, indicating large variance production. The variance production term is dominated by the smallest resolved scales, so even high-order finite-difference schemes are subject to large errors. For positive values of Q_1 , the overprediction actually decreases with increasing filter width. An overprediction of the Q term will increase \bar{Z}^2 and reduce the subfilter variance. Further, these errors are evaluated for a single time step. In practical inhomogeneous calculations, the variance equations evolve spatially and temporally, accumulating errors during the course of the computation. Consequently, the subfilter variance estimated using the VTE will be considerably lower than that found using the STE approach.

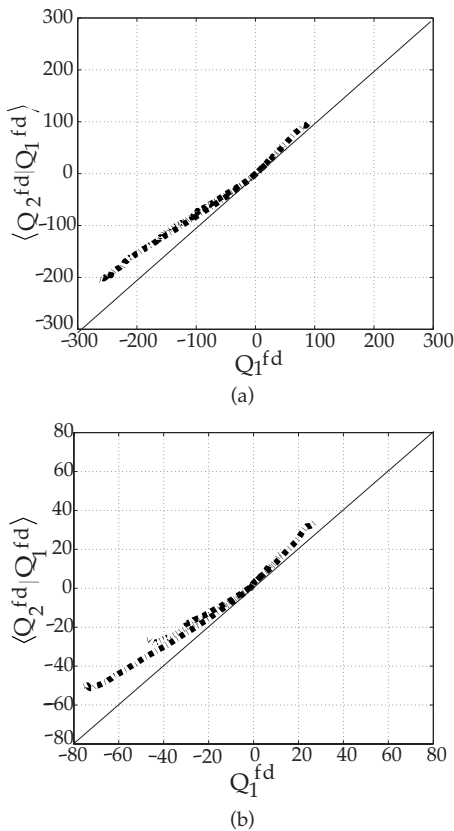


FIG. 8. Conditional mean $\langle Q_2|Q_1 \rangle$ with constant D_t for filter widths of (a) 16η and (b) 64η computed using (dashed line) CD-2, (dotted line) CD-4, and (dashed-dotted line) Padé-6 finite-difference schemes.

It is also worth noting that the choice of numerical method does not significantly alter the qualitative or quantitative nature of the chain-rule errors. For all schemes considered here, the behavior is very similar and the errors are of the same order of magnitude. This result is very similar to the errors observed in the dynamic model formulation discussed earlier. It was also verified that when a spectral method is used for evaluating all derivatives, both forms produce nearly identical P and Q terms, implying that truncation error in the finite-difference schemes plays a crucial role in amplifying the errors. Further, to assess the impact of the diffusivity model on the estimation of Q , a constant diffusivity calculation was performed with the total diffusivity set to a constant value of unity throughout the domain. Figure 8 shows representative plots for two different filter widths. It is readily seen that the trends are very similar to the dynamic eddy diffusivity calculation. These conditional means plotted at different times, with different values of $\langle Z'^2 \rangle$, exhibited identical trends, implying that the results are valid at all times.

In some applications, the nonconservation form of the convective term is preferred. The effects of chain-rule errors on this form were also tested. Results similar to those discussed above were found. Again, only minor differences were observed among the three finite-difference schemes.

C. Equilibrium model for filtered scalar dissipation rate

In addition to the subfilter scalar variance, a number of combustion models (such as flamelet models) require knowledge of the filtered scalar dissipation rate. To specify the filtered scalar dissipation rate, a model for $\bar{\chi}$, defined in Eq. (4), is needed. Making an assumption of local equilibrium leads to the model $\bar{\chi} = 2(D + D_t) \nabla \bar{Z} \cdot \nabla \bar{Z}$. It should be noted that this model follows from setting the production term in the VTE equal to the dissipation rate. The numerical errors in this model stem from the dynamic evaluation of the turbulent diffusivity as well as the calculation of gradients using finite-difference methods. As discussed above, the dynamic procedure partly balances numerical errors in the CDM for the variance, but use of a dynamically calculated turbulent diffusivity has limited effect on the chain-rule errors found in the convective and diffusive terms of the VTE. It would, therefore, be useful to understand the effects of numerical errors on the model for $\bar{\chi}$.

Figure 9 shows the mean value of $\bar{\chi}$ computed using finite-difference approximations, conditioned on $\bar{\chi}$ calculated using spectral methods. The plots clearly indicate that errors in the quantity are substantial over the entire range of true $\bar{\chi}$ values and grow at a faster than linear rate. The underprediction in the gradient term has already been discussed in Sec. IV A. Figure 10 shows the average of the eddy diffusivity calculated using finite differences conditioned on the spectrally computed eddy diffusivity. Finite-difference methods underestimate the eddy diffusivity at all but its lowest values, where it is overpredicted. However, evaluation of $\langle D_t | \mathcal{G}(\bar{Z}) \rangle$, shown in Fig. 11, indicates that high values of D_t correspond to high values of $\mathcal{G}(\bar{Z})$, where finite-difference errors are greatest. It is remarkable that in the calculation of the eddy diffusivity there is little difference among the schemes, indicating that there is cancellation of errors within the dynamic procedure (Fig. 10). However, for none of the numerical schemes is the error cancellation sufficient to compensate for the underprediction of the strain-rate tensor that appears as part of the model. Consequently, the turbulent diffusivity is mostly underpredicted. The gross underprediction of the $\bar{\chi}$ model is a compounded result, involving the underprediction of mixture fraction gradients as well as the eddy diffusivity. The modeled form of $\bar{\chi}$ is similar to the production term in the VTE formulation, Eq. (7). The results for $\mathcal{G}(\bar{Z})$ and D_t suggest that the production term will be underestimated when finite-difference methods are used. It can therefore be concluded, reaffirming the findings of Sec. IV B, that the variance predicted by the finite-difference VTE will always have a lower value than the variance predicted by the spectrally computed VTE.

V. CONCLUSIONS

The interactions of numerical errors with subfilter scalar variance models used in LES of turbulent combustion have been studied using *a priori* analysis methods. The preceding model evaluations show that realizing the predictive value of a model does not necessarily mandate the use of higher-order

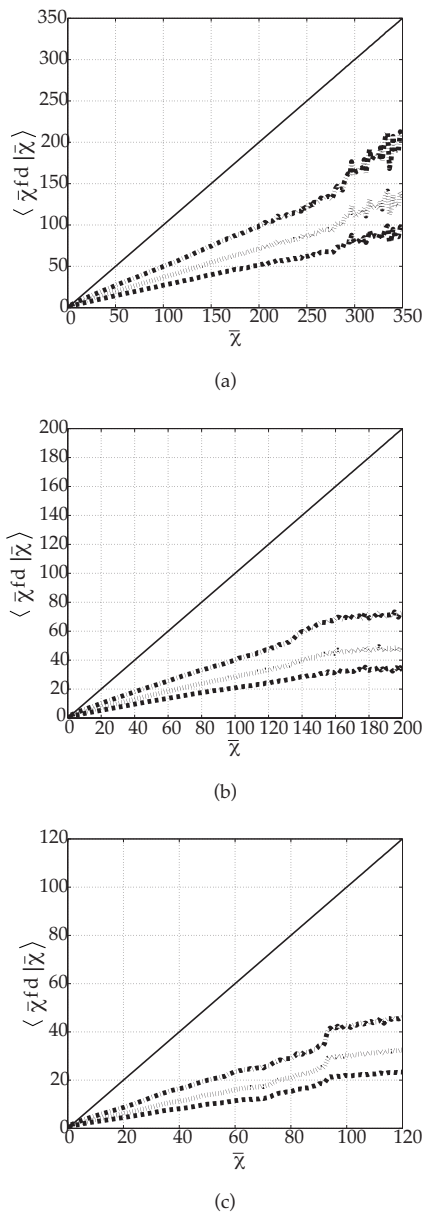


FIG. 9. Conditional average of $\bar{\chi}$ computed using various finite-difference approximations: (dashed line) CD-2, (dotted line) CD-4, and (dashed-dotted line) Padé-6. The conditioning variable is the spectrally computed $\bar{\chi}$. The three plots correspond to three different filter sizes: (a) $\Delta = 16\eta$, (b) $\Delta = 32\eta$, and (c) $\Delta = 64\eta$.

numerics. The analyses were carried out for two categories of subfilter variance models. In the first category, two algebraic models based on the dynamic procedure were evaluated. When model accuracy alone is considered, the BPR dynamic method is superior to the CDM method. Introducing finite-difference effects complicates the picture, particularly at small filter widths where the errors of both models undergo rapid variation. The BPR model shows an advantage in that using higher-order schemes consistently reduces the error. At large filter widths, the CDM model's performance is slightly better, and for either model, there is little difference between the finite-difference methods. Since the relative magnitudes of errors vary as the scalar field decays, the more well-defined behavior of the BPR model is its most attractive

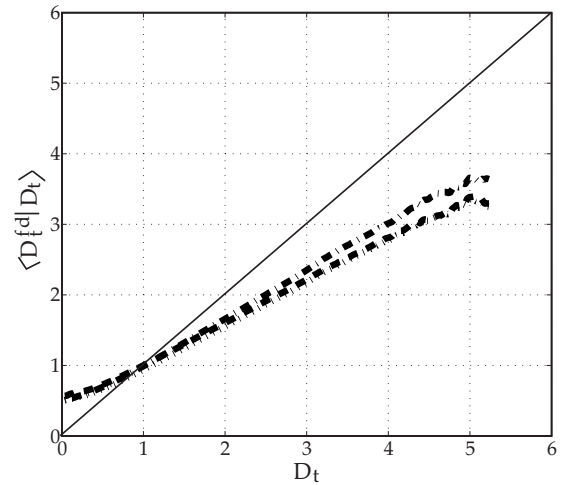


FIG. 10. Conditional average of the eddy diffusivity computed by (dashed line) CD-2, (dotted line) CD-4, and (dashed-dotted line) Padé-6 methods. The conditioning variable is the spectrally computed D_t . The filter width is 32η .

feature. In the category of transport equation based subfilter variance models, the VTE and STE formulations were evaluated. In the limiting case of zero scalar dissipation, the STE model can be shown to reproduce the analytical variance even when solved using finite-difference methods. The VTE lacks this property due to errors induced by discrete approximations to the chain rule. These errors lead to an underestimation of the variance.

Finally, the local equilibrium model for scalar dissipation rate based on the eddy diffusivity and the mixture fraction gradient was considered. In spite of the error cancellation effect in the dynamic procedure, the eddy diffusivity computed using any of the finite-difference schemes is lower in value than that found using spectral methods. Since the mixture fraction gradients are also underpredicted by finite differences, the filtered scalar dissipation rate is subject to

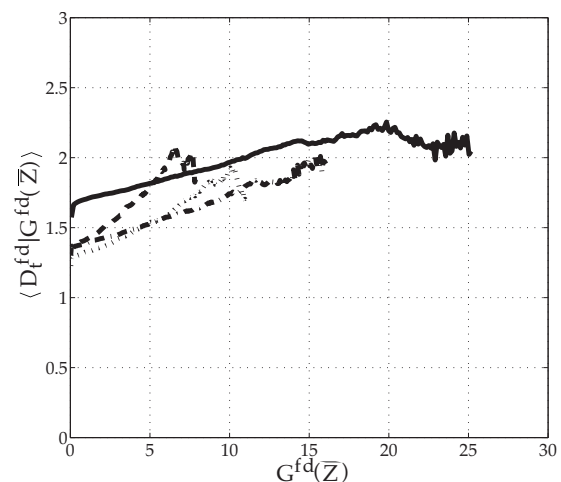


FIG. 11. Conditional average of the eddy diffusivity computed using finite-difference approximations vs the gradient-squared term computed using the same finite-difference schemes: (dashed line) CD-2, (dotted line) CD-4, and (dashed-dotted line) Padé-6. $\Delta = 32\eta$.

large numerical errors. Lower dissipation rates push flames closer to equilibrium and understate the effect of flame strain on the combustion process.

These results indicate that numerical errors play a significant role in the LES modeling of combustion. Through careful model formulation, these numerical effects can be decreased. The STE approach provides a clear example of this process. It should be noted, however, that the results presented here account for the effects of numerical error on model predictions given an accurate filtered scalar field. In a practical LES computation, accumulated errors in the large-scale evolution of the filtered fields could have significant effects on the magnitude of the scalar and velocity gradients. This source of error needs to be considered in order to fully characterize the ramifications of finite-difference errors on the modeling of subfilter quantities.

ACKNOWLEDGMENTS

C.M.K. gratefully acknowledges the support of a National Science Foundation Graduate Research Fellowship. Financial support from NASA through Grant Nos. NNX07AB92A and NNX08AB41A is gratefully acknowledged.

- ¹N. Peters, *Turbulent Combustion* (Cambridge University Press, Cambridge, 2000).
- ²H. Pitsch, "Large-eddy simulation of turbulent combustion," *Annu. Rev. Fluid Mech.* **38**, 453 (2006).
- ³J. Jimenez, A. Linan, M. M. Rogers, and F. J. Higuera, "A priori testing of subgrid models for chemically reacting non-premixed flows," *J. Fluid Mech.* **349**, 149 (1997).
- ⁴A. W. Cook and J. J. Riley, "A subgrid model for equilibrium chemistry in turbulent flows," *Phys. Fluids* **6**, 2868 (1994).
- ⁵C. Jimenez, F. Ducros, B. Cuenot, and B. Bedat, "Subgrid scale variance and dissipation of a scalar field in large eddy simulations," *Phys. Fluids* **13**, 1748 (2001).

- ⁶C. D. Pierce and P. Moin, "A dynamic model for subgrid-scale variance and dissipation rate of a conserved scalar," *Phys. Fluids* **10**, 3041 (1998).
- ⁷G. Balarac, H. Pitsch, and V. Raman, "Development of a dynamic model for the subfilter scalar variance using the concept of optimal estimators," *Phys. Fluids* **20**, 035114 (2008).
- ⁸C. Wall, B. J. Boersma, and P. Moin, "An evaluation of the assumed beta probability density function subgrid-scale model for large eddy simulation of nonpremixed, turbulent combustion with heat release," *Phys. Fluids* **12**, 2522 (2000).
- ⁹S. Ghosal, "An analysis of numerical errors in large-eddy simulations of turbulence," *J. Comput. Phys.* **125**, 187 (1996).
- ¹⁰J. A. Langford and R. D. Moser, "Optimal LES formulations for isotropic turbulence," *J. Fluid Mech.* **398**, 321 (1999).
- ¹¹S. B. Pope, "Ten questions concerning the large-eddy simulation of turbulent flows," *New J. Phys.* **6**, 35 (2004).
- ¹²S. B. Pope, *Turbulent Flows* (Cambridge University Press, Cambridge, 2000).
- ¹³P. J. Colucci, F. A. Jaber, P. Givi, and S. B. Pope, "Filtered density function for large eddy simulation of turbulent reacting flows," *Phys. Fluids* **10**, 499 (1998).
- ¹⁴F. A. Jaber, P. J. Colucci, S. James, P. Givi, and S. B. Pope, "Filtered mass density function for large-eddy simulation of turbulent reacting flows," *J. Fluid Mech.* **401**, 85 (1999).
- ¹⁵V. Raman and H. Pitsch, "A consistent LES/filtered-density function formulation for the simulation of turbulent flames with detailed chemistry," *Proc. Combust. Inst.* **31**, 1711 (2007).
- ¹⁶M. Germano, U. Piomelli, P. Moin, and W. H. Cabot, "A dynamic subgrid-scale eddy viscosity model," *Phys. Fluids A* **3**, 1760 (1991).
- ¹⁷S. S. Girimaji and Y. Zhou, "Analysis and modeling of subgrid scalar mixing using numerical data," *Phys. Fluids* **8**, 1224 (1996).
- ¹⁸P. Moin, *Fundamentals of Engineering Numerical Analysis* (Cambridge University Press, Cambridge, 2000).
- ¹⁹A. G. Kravchenko and P. Moin, "On the effect of numerical errors in large eddy simulations of turbulent flows," *J. Comput. Phys.* **131**, 310 (1997).
- ²⁰K. Alvelius, "Random forcing of three-dimensional homogeneous turbulence," *Phys. Fluids* **11**, 1880 (1999).
- ²¹V. Eswaran and S. B. Pope, "Direct numerical simulations of the turbulent mixing of a passive scalar," *Phys. Fluids* **31**, 506 (1988).
- ²²C. D. Pierce and P. Moin, "Progress-variable approach for large-eddy simulation of non-premixed turbulent combustion," *J. Fluid Mech.* **504**, 73 (2004).